# Thermal mode instabilities in high power fiber lasers

*A Project Report*

*submitted by*

**Thejna Ros Joseph**

*in partial fulfilment of requirements*

*for the award of the degree of*

**MASTER OF TECHNOLOGY**


**DEPARTMENT OF ELECTRICAL ENGINEERING**

**INDIAN INSTITUTE OF TECHNOLOGY MADRAS**

**MAY 2017**

# THESIS CERTIFICATE

This is to certify that the thesis titled **Thermal mode instabilities in high power fiber lasers**, submitted by **Thejna Ros Joseph,** to the Indian Institute of Technology, Madras for the award of the degree of **Master of Technology** (Photonics) in Electrical Engineering, is a bonafide record of the research work done by her under my supervision. The contents of the thesis, in full or in parts, have not been submitted to any other Insitute or University for the award of any degree or diploma.

**Prof. Anil Prabhakar**
Research Guide
Professor
Dept. of Electrical Engineering
IIT Madras - 600036

Place: Chennai

Date : 2$^{nd}$ May 2017

# Acknowledgement

I express my sincere gratitude to Prof. Anil Prabhakar, Professor, Department of Electrical Engineering, Indian Institute of Technology, Madras, Dr. Deepa Venkitesh, Associate Professor, Department of Electrical Engineering, Indian Institute of Technology, Madras, and Dr. Balaji Srinivasan, Associate Professor, Department of Electrical Engineering, Indian Institute of Technology, Madras, who have been constant sources of inspiration and guidance throughout the execution of my research work.

I thank all the Photonics (EE5) faculities for their valuable support throughout my work.

I would like to thank Dr. Aditi Ghosh , Yusuf Panbiharwala, Manas Srivasthava and Varun Kelkar for their resourceful inputs to my work. I also thank all my lab members and friends for their support throughout the research period.

**Abstract**

KEYWORDS : Thermal mode instability; Thermo-optic effect; Beam propagation method; Steady-state thermal solver; Parallel computing

In high power fiber lasers, presence of high power can induce non-linear effects and thermo-optic effects which result in modifying the refractive index profile.The objective of the project is to simulate the consequences of thermo-optic effect on fiber modes and modal instabilities at the output. Study of thermal mode instabilities can help in proposing better designs to overcome this bottleneck. Mode instabilities occurring in optical fibres while guiding high power signal due to thermo-optic effect is simulated using Python and performance is improved using GPU computing. The model shows that power transfer between the fundamental and higher-order modes of the fiber can be induced by interaction through the thermo-optic effect, leading to thermal mode instabilities.

# Contents

# List of Figures

# List of Tables

# Chapter 1

# Introduction

Fibers have always been amenable to engineering and have high level of functionality. Fiber lasers combine high average powers, beam quality, small footprint with high efficiencies. Currently, fiber lasers hold a vast share of the industrial applications market. High power fiber lasers are used in variety of applications in communication and defense applications. The low power fiber amplifiers efficiently used in fiber-based internet can be scaled massively as industrial laser frontrunner[1]. Experimental research in power scaling have come a long way but currently, face with the power bottlenecks. Clear trend is that thermal effects, non-linear effects and damage are becoming key limiting factors for an increasing number of devices. Extensive theoretical study is required for understanding and mitigation of this performance boundaries.

## 1.1 High power fiber lasers

Lasers are based on the amplification of signal by stimulated emission, include an active medium to provide gain, an optical cavity to enhance and control the optical field and a pumping source to provide the energy. Details of these features decide the laser performance, the power scaling capabilities, stability, footprint and cost. Fiber lasers have the rare-earth doped fibers as the active medium. The brightness, which determines the acheivable power density on the target is exceptionally high in fiber lasers. Tunability of the fiber is an attribute of the amorphous nature of glass host in fiber core which allows inhomogeneous broadening of emission and aborption spectra. Furthermore, this allows efficient use fiber lasers in ranges from continous wave to ultra-short pulses[2].

Better thermal management due to large surface to volume ratio of the fibers, superior beam quality and stability due to controlled spatial distribution of the signal,

provided by the continuous guidance, small quantum defect, as well as, low cavity and transmission losses and small footprint contribute to superior performance of fiber lasers over solid state lasers[3]. Multiple stages of solid-state lasers can be used as seeds for the fiber lasers in high power configurations. Average power scaling through master oscillator power amplifier (MOPA) and cascaded amplifier configurations are made possible by high gain of fiber amplifier[1]. The high-power handling capability offered by the geometry of the fiber has led the unparalleled progress of fiber laser systems to multi-kW industrial systems.

### 1.1.1 Classic Limitations & Solutions :

Generally, coupling of high power pump to attain high power lasing is difficult due to small dimensions of core which is required for single mode condition, so as to avoid dispersion losses. Double clad fiber solves this problem by coupling high power pump light into the inner cladding, where the pump is guided between inner and outer cladding. Moreover, this increases the cross-section reducing the brightness and including multimode effects.

Further drawback in having a long and thin gain medium is nonlinear optical degradation caused by high intensity signals resulting in effects like stimulated brillouin scattering (SBS), stimulated Raman scattering (SRS), self phase modulation and self focusing. SBS is caused by interaction of light and acoustic waves propagating in the fiber. Above a sharp power threshold energy is transferred from signal to frequency downshifted backward propagating beam. SRS is caused by interaction of light with molecular vibrations in glass fiber resulting in frequency downshifted beam in all directions. These effects can be mitigated using spectral filtering. SPM occur due to quasi instantaneous refractive index modification by Kerr effect which modifies the phase of the light wave through non-linear variation of optical path. Unlike other non-linear effects that limit the average power, self focusing limits the peak power, which thus determines the ulitimate limit for the power scaling[4].

The product of peak intensity and fiber length need to be minimised to reduce non-linear effects. The peak intensity can be reduced by increasing the mode field diameter. This will in turn increase the pump absorption and the length of the amplifier can be reduced. Non-linear effects reduces with reduction in the fiber length. However, large core area in these fibers, to lower intensity below the nonlinearity thresholds leads to beam degradation through multimode guiding.

## 1.2 Thermal effects

Thermal effects in fiber was not a major concern for a long time unlike in the solid-state lasers, owing to the good thermal properties of optical fibers. Nevertheless, with recent researches like the Ytterbium doped fiber lasers power scalable to 10 kW of power, limitations due to thermal effects is significant. Thermal effects can create the refractive index profile changes due to thermo-optic effect affecting the waveguiding. Thermal mode instabilities (TMI) limit maximum average power obtainable from fiber lasers. Improved brightness and larger cores have made study on thermal effects more important in the current scenario.

Due to proximity of pump and signal wavelength, ytterbium is a very efficient laser ion. The difference determines the surplus heat produced in the medium, which triggers the thermo-optic effects. High yetterbium concentrations lead to absorption of pump within first few meters of fiber. For certain wavelengths, the transmission and scattering losses accumulate causing photodarkening which leads to beam degradation limiting the lifetime of the fiber laser. Photodarkening manifests itself as a temporal increase in broadband absorption centered at visible wavelengths[5]. Development of new silica-based glass hosts have helped in avoiding photodarkening.

Future innovations in materials and fiber designs, following the spectacular progress in their performance so far, are expected to continue pushing the performance boundaries with new radical fiber laser solutions. This necessitates the need to go for in depth understanding of high power fiber laser dynamics.

### 1.2.1 Thermal mode instability (TMI)

Mode instabilities is the current challenge faced in power scaling as it restricts the maximum average power rather than capping the peak intensity. In high power fiber lasers, operating above power levels of hundreds of Watts exhibit instbilities in beam. When pump power exceeds certain threshold the beam quality drastically degrades. Beam quality degradation at the output, in large mode area fibers used in high power applications, is due to multimode guiding. Mode instability refers to fluctuations in otherwise highly stable output beam profile of the fiber amplifiers beyond an average power threshold.

Experimentally, these instabilities were observed in Yb-doped amplifiers pumped at 976 nm and with signal in the range 1030-1080 nm. Reported instability thresholds fall in the range of 100 W to 2500 W[6]. Beam shape starts fluctuating once the average power threshold is exceeded. It retains stability, when the power is lowered

again. Thus a stable regime, a transition region and a chaotic regime was identified for the output beam.

Above a threshold power, beam shape fluctuates on millisecond scale. These beam fluctuations are said to occur due to periodic modulation of refractive index profile of active fiber through thermo-optic effect and/or gain in the medium through Kramer-Kronig relation. Unlike other instabilities found in similar systems, TMI in fiber can be mitigated through efficient waveguide design. This project aims at simulating output signal intensity profile in high power fiber lasers and to study the fluctuations of normally stable high quality beams emitted by high power lasers observed over a certain average power threshold.

This report summarizes the attempt to simulate thermal mode instabilities in high power lasers. Chapter 2 discusses about the physical orgin of TMI. Different phenomena that might result in power transfer between the modes which result in beam fluctuation and instability are discussed. Chapter 3 describes the assumptions used in the algorithm and the equations used. Computer implementation and algorithm is explained in chapter 4. The numerical experiments done using the model is described in chapter 5. It includes the verification results and simulation output from the model. Chapter 6 summarizes the model and discuss about the future scope. Appendix on the analytical solutions of thermal diffusion equation in radial direction is also included.

# Chapter 2

# Physical Orgin of TMI

Instability within a system is characterized by the fluctuations between two or more internal states of the system. Thermal mode instability manifests itself as rapid output beam fluctuations when the fundamental mode and first higher order mode (HOM) interact. Large mode area fibers allow multimode guiding resulting in coherent interference of modes, creating a quasi-periodic interference intensity pattern. This would result in a corresponding inversion and temperature pattern which through thermo-optic would cause a quasi-periodic refractive index variation along the length of the fibre. This refractive index grating has adequate period to transfer power between modes.

Few publications have also proposed an additional phase shift between the refractive index grating and the interference pattern for coupling of modes[9]. The cause of this additional phase shift is a much debated hypothesis for explaining the occurrence of the instabilities. It is proposed that when HOM is frequency downshifted with respect to the fundamental mode by a few kHz, a moving interference intensity pattern is formed. The delayed thermal gratings due to the finite thermal conductivity of silica creates the neccessary condition for the energy transfer. On the other hand, presence of non-adiabatic waveguide changes which would result in a phase shift between index profile and beam intensity is offered as an alternative explanation.

The numerical models usually implemented for each of this proposed theories include various assumptions to reduce the computational intensity. Our model assumes steady-state thermal grating without initial phase shift between the modes. Power transfer between the modes has been studied. The various phenomena that occur in high power lasers that prefer specific modes and thus dominate the power content in different modes are discussed below.

## 2.1 Thermal - induced self focusing

The variation of refractive index of waveguide with temperature (neglecting Kramer-Kronig effect) is given by eq.(2.1),

$$n^2(x,y) = n_{wg}^2(x,y) + 2n_0\frac{dn}{dT}\Delta T(x,y) \tag{2.1}$$

where $n_{wg}$ is the refractive index of the cold fiber, $\frac{dn}{dT}$ is the thermo-optic coefficient ($1.2\text{x}10^{-5}K^{-1}$). When the fiber heats up, the temperature increase causing a positive temperature difference $\Delta$T (x, y, z), which lead to increase in the refractive index.

In high power fiber lasers, the gain medium is hotter on the beam axis, compared to the outer regions, causing a transverse gradient of refractive index. The refractive index would increase in the middle, compared to the outer edges, favouring more power confinement in the fundamental mode as it propagate along the length. As the beam propagates along the length of the fiber, this cause self-focusing as the high refractive index in the middle of the fiber leads to guiding of signal with smaller mode field diameter. Reduction in the beam further increases the intensity which increases the self-focusing of the beam.

## 2.2 Gain Saturation

Gain in fiber amplifiers is a result of dopant ions in the fiber. The inversion level in the fiber amplifier is due to population inversion of the dopant ions. The inversion level depends on the power in pump and signal. As the signal power increases or pump decreases, the inversion level reduces thereby reducing the gain of the amplifier. As the signal power increases, amplifier saturates and causing reduction in amplification, thus causing the gain to saturate.

The gain profile is dependant on the signal power profile. At a given spatial position, the medium sees the superposition of all modes present there. With same frequency in all modes, the medium does not differentiate with them. Thus the modes avail similar gain at every spatial position. The difference in gain available for different modes come from the different spatial profile of the modes. Since the power in fundamental mode is high, in usual cases it dominates the gain. Near the beam axis, gain saturates faster due to high power in fundamental mode. At regions were power in modes are comparable, gain saturation is much slower. When the intensity at the beam axis reaches the saturation intensity, the amplification for fundamental mode would be less than that of the higher order modes. In this case, the higher order modes are

preferred. The figure in Fig.2.1 shows the gain curve for a pump power of 300 W, with markers for saturation signal power and input powers of fundamental and higher order modes used in the simulation model. The pump power is already in the saturation regime. The signal input powers in all modes are also saturated making effects of saturation regime inevitable.

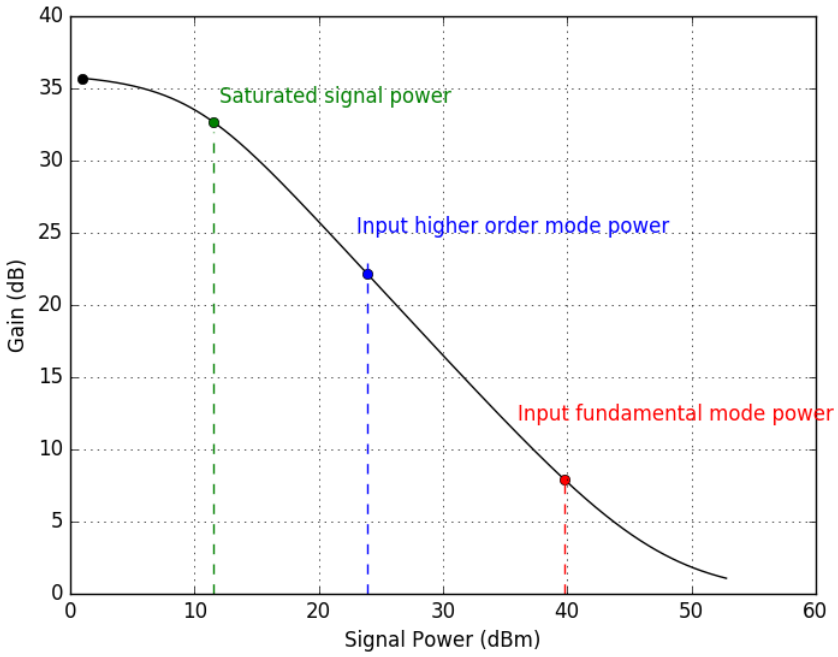


Figure 2.1: Variation in gain for fundamental and higher order modes

Thermal effect along with gain saturation can cause power transfer. Power transfer require the nonzero overlap between the modes of the fiber which occur when the refractive index is perturbed by the thermal profile.

## 2.3 Thermal grating

Transfer of power between otherwise non-interacting modes of fiber can be possible in presence of temporally varying thermal gratings. Variations in electric tensor is considered as a perturbation that couples the unperturbed normal modes of propagation of the structure. When the dielectric constant is perturbed, the unperturbed modes are no longer eigenmodes of the perturbed system, allowing them to transfer energy.

The multimode waveguide has intensity variations along the length of fiber due to coherent interference of the mode. These variation result in a corresponding inversion

profile which heats up the medium, causing index gratings along the length. The beam does not diffract with its own intensity due to lack of phase matching[8]. But when the grating period matches the beat length of intensity variations, the modes couple energy.

Our model uses beam propagation method along with steady-state thermal solver to study these phenomena along the length of the fiber. The model which works in saturation regime, in presence of thermal induced grating simulates self-focusing and gain saturation, and coupling of the perturbed modes. The theoretical background for model is disucussed in detail in the next chapter.

# Chapter 3

# Beam propagation method

A 3D beam propagation model (BPM), including laser gain for spatial evolution of signal fields along with 2D steady state thermal solver is used for studying the power transfer between modes of fiber and beam fluctuations at the output.

For BPM, each propagation step is taken as a fraction of intermodal beat length, taking care that there is enough sample points in each beat length for tracing the parameter varitions along length. Since the speed of light is very much higher than the speed of thermal diffusion, rate calculations can be done multiple times before a thermal calculation.

## 3.1 Model assumptions and equations

Signal is launched into the core while the pump is guided by the inner cladding in a double clad fiber. A constant pump power profile can be considered as multiple modes are allowed for the pump in the inner cladd due to large numerical aperture. The signal modes are calculated as the solutions of scalar wave equation. A lossless and perfectly reflecting optical boundary condition is used. A subgrid around the core can be used for FDM calculations of scalar wave equations and rate equations, since the signal is confined only in the core were the doped ions are present

### 3.1.1 Scalar wave equations

Scalar optical wave equation valid for a weakly-guiding fiber [9] is given by eq.(3.1),

$$\nabla^2 E(x,y,z) + n^2(x,y,z)k_0^2 E(x,y,z) = 0 \tag{3.1}$$

where $k_0 = \frac{\omega}{c}$, free space wave vector, n(x,y,z) is the refractive index profile and

E(x,y,z) is the electric field distribution.

Invoking slowly varying envelope and paraxial approximation, we have eq.(3.2),

$$[-2i\beta\frac{\partial}{\partial z}+\nabla_t^2+n^2(x,y,z)k_0^2-\beta^2]E(x,y,z)=0 \tag{3.2}$$

where $\beta$ is the wave vector describing rapid oscillations in propagation direction, $\nabla_t^2$ is the transverse Laplacian operator.

Setting $\frac{\partial E}{\partial z}=0$ and $\frac{\partial n}{\partial z}=0$ , yields eq.(3.3),

$$[\frac{\partial^2}{\partial x^2}+\frac{\partial^2}{\partial y^2}+n^2(x,y)k_0^2]E(x,y)=\beta^2E(x,y) \tag{3.3}$$

Applying FDM, we have eq.(3.4),

$$\frac{E(x+\Delta x,y)+E(x,y+\Delta y)+E(x-\Delta x,y)+E(x,y-\Delta y)-4E(x,y)}{\Delta x^2}+n^2(x,y)k_0^2E(x,y)=\beta^2E(x,y) \tag{3.4}$$

we obtain an eigen equation which is solved using ARPACK package which use iterative Arnoldi method to find the first three eigenvalues $\beta_1$, $\beta_2$, $\beta_3$ and corresponding eigenvectors $e_1(x,y)$, $e_2(x,y)$, $e_3(x,y)$. $e_i(x,y)$ is normalized electric field corresponding to $i^{th}$ mode of the fiber. The second and third modes are degenerate higher order modes. The power in other high order modes are assumed to be negligible. Also, bend-induced mode distortion and other bending losses are not accounted for.

**Renormalization**

The normalized electric field profiles are renormalized using eq.(3.5),

$$P_{si}(x,y,z_0)=P_i(z_0)|e_i(x,y,z_0)|^2 \tag{3.5}$$

where $P_{si}(x,y,z_0)$ is the signal power profile, $P_i(z_0)$ is the total power and $e_i(x,y,z_0)$ is the normalized electric field profile for $i^{th}$ mode at length $z_0$ of fiber.

After obtaining $e_i(x,y)$ as the eigen vector of the scalar wave equation, envelope is allowed to slowly vary along the length of the fiber according to the rate equations in the fiber amplifer.

### 3.1.2 Gain and heat deposition

Gain is instantaneously determined by the local pump, signal intensities in the fiber.

The intensity profile of pump and signal at $z_0$ is given by eq.(3.6), eq.(3.7) respectively,

$$I_p(x,y,z_0) = \frac{P_{pump}(z_0)}{Area_{innercladd}} \tag{3.6}$$

$$I_s(x,y,z_0) = \frac{|\sum_{i=1}^{3} \sqrt{P_i(z_0)} e_i(x,y,z_0) e^{j\beta_i z_0}|^2}{\Delta x \Delta y} \tag{3.7}$$

An active media for which the atomic energy level populations are determined by two-level rate equations is assumed. The doped region is assumed to be circular and uniform. The excited ion population is given by eq.(3.8),

$$N_2(x,y,z_0) = N_{tot}(x,y,z_0) \frac{\frac{I_s(x,y,z_0)\sigma_{as}\tau}{h\nu_s} + \frac{I_p(x,y,z)\sigma_{ap}\tau}{h\nu_p}}{1 + \frac{I_s(x,y,z_0)(\sigma_{as}+\sigma_{es})\tau}{h\nu_s} + \frac{I_p(x,y,z_0)(\sigma_{ap}+\sigma_{ep})\tau}{h\nu_p}} \tag{3.8}$$

The ground state population is given by eq.(3.9),

$$N_1(x,y,z) = N_{tot}(x,y,z) - N_2(x,y,z) \tag{3.9}$$

Assuming negligible attenuation and scattering losses, the gain profile for the signal and pump is given by eq.(3.10), and eq.(3.11) respectively,

$$g_s(x,y,z) = N_2(x,y,z)\sigma_{es} - N_1(x,y,z)\sigma_{as} \tag{3.10}$$

$$g_p(x,y,z) = N_2(x,y,z)\sigma_{ep} - N_1(x,y,z)\sigma_{ap} \tag{3.11}$$

Power profile of $i^{th}$mode after propagating dz length, changes according to eq.(3.12),

$$P_{si}(x,y,z_0+dz) = P_{si}(x,y,z_0)(1+g(x,y,z_0)dz) \tag{3.12}$$

Total power in $i^{th}$ mode is given by eq.(3.13),

$$P_i(z_0+dz) = \int\int P_{si}(x,y,z_0+dz)dxdy \tag{3.13}$$

The total pump power after dz propagation step is given by eq.(3.14),

$$P_{pump}(z_0+dz) = P_{pump}(z_0) + \int\int (I_p(x,y,z_0)g(x,y,z_0)dz)dxdy \tag{3.14}$$

The heat load is calculated neglecting the contribution from the spontaneous emission is calculated using eq.(3.15)[10],

$$Q(x,y,z_0+dz) = (\frac{\nu_p}{\nu_s} - 1)(I_s(x,y,z_0+dz) - I_s(x,y,z_0)) \tag{3.15}$$

The diffusion of heat in the fiber is implemented using the heat diffusion equation.

### 3.1.3 The steady-state heat equation

The heat equation is given by eq.(3.16),

$$\frac{\partial T(x,y,z,t)}{\partial t} = \frac{K}{\rho C}\nabla^2 T(x,y,z,t) + \frac{1}{\rho C}Q(x,y,z,t) \tag{3.16}$$

where T is the temperature, Q is the heat power density, K is the thermal conductivity, $\rho$ is the mass density and C is the heat capacity within the fiber.

The steady-state heat equation with a heat source (inhomogeneous case) is a Poisson's equation eq.(3.17),

$$\nabla^2 T(x,y,z_0) = \frac{-Q(x,y,z_0)}{k} \tag{3.17}$$

The thermal properties of the system of the system is considered constant in the cross-section. Dirichlet boundary condition is applied in x and y direction as the fiber is surrounded by a heat sink. The diffusion in z direction can be neglected as the heat sink in radial direction is closer than thermal propagation step. Free convection is assumed to be an order of magnitude less efficient than conduction for dissipating heat from the optical fiber. Thus we have eq.(3.18),

$$\frac{\partial^2 T(x,y,z_0)}{\partial x^2} + \frac{\partial^2 T(x,y,z_0)}{\partial y^2} = \frac{-Q(x,y,z_0)}{K} \tag{3.18}$$

Applying finite difference method, we have eq.(3.19),

$$\frac{T(x+\Delta x,y,z_0)+T(x-\Delta x,y,z_0)-2T(x,y,z_0)}{\triangle x^2} + \frac{T(x,y+\Delta y,z_0)+T(x,y-\Delta y,z_0)-2T(x,y,z_0)}{\triangle y^2} = \frac{-Q(x,y,z_0)}{K} \tag{3.19}$$

where Q is the heat power density, K is the thermal conductivity .

Since it is assumed that the only source of heat in the fiber is due to amplfication in fiber, the heat source is present in the core only.

The $\Delta T(x,y,z_0)$ obtained as the solution of 2D heat equation changes the refractive index profile through thermo-optic effect.

### 3.1.4 Thermo-optic effect

The refractive profile of the waveguide is influenced by the gain within the core and thermally induced refractive index profile as in eq.(3.20),

$$n^2(x,y,z_0+dz) = n^2(x,y,z_0) + in(x,y,z_0)g(x,y,z_0) + 2n(x,y,z_0)\frac{dn}{dT}\Delta T(x,y,z_0) \quad (3.20)$$

where the refractive index is changed by the Kramer-Kronig and thermo-optic effect. But the influence of Kramer-Kronig can be neglected as the change is relatively small compared to the thermo-optic effect.

### 3.1.5 Perturbed modes

The change in dielectric constant is considered as a perturbation and the modes for the perturbed refractive index profile is calculated again using the scalar wave equation after every thermal propagation step. The power transferred into the perturbed modes is calculated using the overlap factors between both the set of modes using eq.(3.21),

$$\Gamma_{ij} = \frac{|\int\int e_i(x,y,z_0)e_j(x,y,z_0+dz)dxdy|^2}{\int\int |e_i(x,y,z_0)|^2 dxdy \int\int |e_j(x,y,z_0+dz)|^2 dxdy} \quad (3.21)$$

where i and j vary from 1 to 3.

The power transferred to $i^{th}$mode is given by eq.(3.22),

$$P_i(x,y,z_0+dz) = \sum_{j=1}^{3} \Gamma_{ij} P_j(x,y,z_0) \quad (3.22)$$

with $z_0$ varied along the length of the fiber.

No material scattering loss and bending loss is assumed. Pump and signal linewidth is considered to be negligible.

The algorithm followed in the model, computer implementation of the model FDM methods and scope of improvement in performance using parallel programming is discussed in the next chapter.

# Chapter 4

# Computer Implementation

A 3D beam propagation model along with 2D steady state thermal solver is used to study the power transfer between modes of fiber and beam fluctuations at the output. This model has optical propagation step of 100 $\mu$m for rate calculations and thermal propagation step of 4 mm. A 2D grid of 383 x 383 was considered for thermal calculations in cross-section of the fiber. The mode calculations use a subgrid of 95 x 95 around the core.

At the start of simulation, initial refractive index profile, temperature distribution and input pump and signal powers were specified. 95% of the input signal power is assumed to be in the fundamental mode and the rest in the higher order modes. The power in other higher modes are considered negligible. Finite difference method is used to solve the scalar wave equation. ARPACK package is used to find the sparse linear system solution for the eigen equation.

The steady state rate equations are solved to find the fraction of excited dopant profile and thus track the increase in power profiles with gain. The surplus energy absorbed by the active medium is considered as the heat source for the thermal solver with calculates the temperature difference along the cross-section of fiber with a Dirichlet boundary condition. This is considered to perturb the dielectric constant profile which affects the power coupling between modes.

A flowchart of the algorithm used for the model is given below. The matrix formalism for the input sparse matrix to ARPACK package and eigensolution retrieval is explained briefly.

## 4.1 Algorithm

The following algorithm was used in the model.

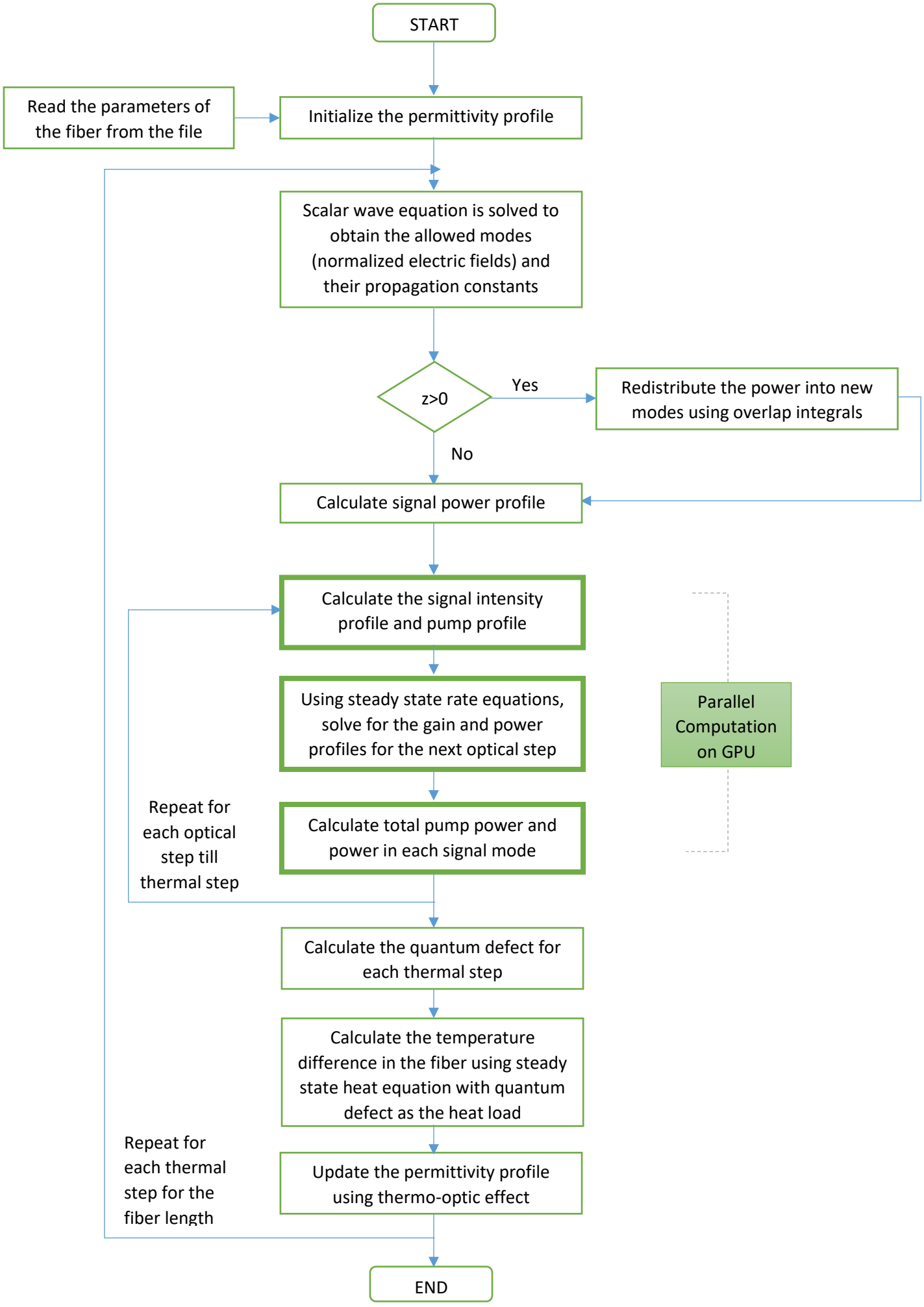
START
Read the parameters of the fiber from the file
Initialize the permittivity profile
Scalar wave equation is solved to obtain the allowed modes (normalized electric fields) and their propagation constants
z>0
Yes
Redistribute the power into new modes using overlap integrals
No
Calculate signal power profile
Calculate the signal intensity profile and pump profile
Using steady state rate equations, solve for the gain and power profiles for the next optical step
Calculate total pump power and power in each signal mode
Repeat for each optical step till thermal step
Parallel Computation on GPU
Calculate the quantum defect for each thermal step
Calculate the temperature difference in the fiber using steady state heat equation with quantum defect as the heat load
Update the permittivity profile using thermo-optic effect
Repeat for each thermal step for the fiber length
END

### 4.1.1 Matrix formalization

The scalar wave equation is an eigen equation of the form,

$$AX = \lambda X \tag{4.1}$$

where A is the operator matrix , which when diagonalized and solved would yield the set of eigenvalues and corresponding eigenvectors.

Applying FDM to eq.(3),

$$\frac{E_{i+1,j}(x,y)+E_{i-1,j}(x,y)-2E(x,y)}{\Delta x^2}+\frac{E_{i,j+1}(x,y)+E_{i,j-1}(x,y)-2E_{i,j}(x,y)}{\Delta y^2}+n_{i,j}^2(x,y)k_0^2E_{i,j}(x,y)=\beta^2E_{i,j}(x,y) \tag{4.2}$$

where i and j are indices of matrix.

$$\begin{bmatrix}
\frac{-2}{\Delta x^2}+\frac{-2}{\Delta y^2}+n_{11}^2k_0^2 & \frac{1}{\Delta x^2} & \dots & \dots & \frac{1}{\Delta y^2} & 0 & 0 & \dots & \dots & 0 \\
\frac{1}{\Delta x^2} & \frac{-2}{\Delta x^2}+\frac{-2}{\Delta y^2}+n_{22}^2k_0^2 & \dots & \dots & 0 & \frac{1}{\Delta y^2} & 0 & \dots & \dots & 0 \\
0 & \frac{1}{\Delta x^2} & \dots & \dots & 0 & 0 & \frac{1}{\Delta y^2} & \dots & \dots & 0 \\
\dots & \dots & \dots & \dots & \dots & \dots & \dots & \dots & \dots & \dots \\
\dots & \dots & \dots & \dots & \dots & \dots & \dots & \dots & \dots & \dots \\
\frac{1}{\Delta y^2} & 0 & \dots & \dots & 0 & 0 & 0 & \dots & \dots & 0 \\
0 & \frac{1}{\Delta y^2} & \dots & \dots & 0 & 0 & 0 & \dots & \dots & \frac{1}{\Delta y^2} \\
0 & 0 & \dots & \dots & 0 & 0 & 0 & \dots & \dots & 0 \\
\dots & \dots & \dots & \dots & \dots & \dots & \dots & \dots & \dots & \dots \\
\dots & \dots & \dots & \dots & \dots & \dots & \dots & \dots & \dots & \dots \\
0 & 0 & \dots & \dots & 0 & \frac{1}{\Delta y^2} & 0 & \dots & \dots & \frac{-2}{\Delta x^2}+\frac{-2}{\Delta y^2}+n_{NxNy}^2k_0^2
\end{bmatrix}
\begin{bmatrix} E_{11} \\ E_{12} \\ E_{13} \\ \vdots \\ \vdots \\ E_{21} \\ E_{22} \\ \vdots \\ \vdots \\ E_{NxNy-1} \\ E_{NxNy} \end{bmatrix}
= \beta^2
\begin{bmatrix} E_{11} \\ E_{12} \\ E_{13} \\ \vdots \\ \vdots \\ E_{21} \\ E_{22} \\ \vdots \\ \vdots \\ E_{NxNy-1} \\ E_{NxNy} \end{bmatrix} \tag{4.3}$$

The electric field in each grid corresponding to the cross-section of the fiber is mapped into a column matrix. The discretized wave equation is translated into matrix formalism where the basis electric field profiles are given by this column matrices. The operator matrix will have the whole information about the system. The operator A turns out to be a sparse matrix, with non-zero elements in the main diagonal and -1, 1, *Nx* and -*Nx* diagonals. The coefficients of $E_{i,j}(x,y)$ are the main diagonal elements, $E_{i-1,j}(x,y)$ and $E_{i+1,j}(x,y)$ are the lower and upper diagonals respectively. $E_{i,j-1}(x,y)$ will be present as the $Nx^{th}$ lower diagonal and $Nx^{th}$ upper diagonal corresponds to $E_{i,j+1}(x,y)$. This is because, in our mapping, the 2D matrix of the cross-section is mapped into the column matrix for the electric field profile in row major form. So, the $(j-1)^{th}$ and $(j+1)^{th}$ will correspond to $Nx^{th}$ lower and upper diagonals.

In our model, since$\Delta x = \Delta y$ is considered, the eigen equation is simplified to,

$$\frac{E_{i+1,j}(x,y)+E_{i,j+1}(x,y)+E_{i-1,j}(x,y)+E_{i,j-1}(x,y)-4E_{i,j}(x,y)}{\Delta x^2}+n_{i,j}^2(x,y)k_0^2E_{i,j}(x,y)=\beta^2E_{i,j}(x,y) \tag{4.4}$$

#### 4.1.1.1 ARPACK package

The eigen equation which is solved using ARPACK package which use iterative Arnoldi method to find the first three eigenvalues. In numerical linear algebra, the Arnoldi iteration is an iterative eigenvalue algorithm. It gives partial results after small number of iterations unlike the direct methods. Arnoldi iteration is a large sparse matrix algorithm. It does not access the elements of the matrix directly, but rather makes the matrix map vectors and makes its conclusions from their images[1]. Arnoldi iteration used for solving sparse non-Hermitian matrix while Lanczos iteration is for the Hermitian matrix.

ARPACK is a Fortran package which provides routine for quickly finding eigenvalues and eigenvectors of large sparse matrices. All of the functionality provided in ARPACK is contained within the two high-level interfaces scipy.sparse.linalg.eigs and scipy.linalg.eigsh. eigs provides interfaces to find the eigenvalues/vectors of real or complex nonsymmetric square matrices, while eigsh provides interfaces for real-symmetric or complex -hermitian matrices.

To increase the speed of mode calculations, eigen values are calculated around guess, $\beta^2 = (\frac{2\pi}{\lambda} max(n))^2$. Use of guess eigenvalue provides a six times performance improvement. The solver calculates first three eigenvalues $\beta_1$, $\beta_2$, $\beta_3$ and corresponding eigenvectors $e_1(x,y,)$, $e_2(x,y)$, $e_3(x,y)$. $e_i(x,y)$ is normalized electric field corresponding to $i^{th}$ mode of the fiber. The second and third modes are degenerate higher order modes.

The optical power profile and propagation, determined by this electric field profile is spatially independent. This facilitates use of parallel computing techniques to improve the performance.

## 4.2 Parallel Computing

Parallel programming is a useful approach to program computationally heavy simulations. Parallel computing is the computation in which many calculations or the execution of processes are carried out simultaneously. Parallelism can be bit-level, instruction-level or task level. Instruction level parallelization is done in absence of data dependency. In contrast to data parallelism, where same calculation is performed, task parallelism have different processors, each allocated with a sub-task.

Classes of parallel computing include multi-core computing, distributed computing, cluster computing, general- purpose computing on graphic processor units (GPGPU)

etc. GPUs are heavily optimized for computer graphics processing, dominated by data parallel operations. Accelerated computing use both CPU and GPU to run the work. In such programs, CPUs act as the host and call GPU to run heavily loaded part of the code. CPUs are optimized for latency and GPUs are throughput optimized. GPUs can be used best for parallel computing of independent and countable steps. Performance of the program can be increased using accelerate libraries, further by high level parallel programming directives like OpenACC or by low level, less portable languages like CUDA or combinations of them.

PyOpenCL is used here for the implementation of optical propagation in the algorithm for thermal mode instability using Intel Corporation second generation core processor GPU for improved performance.

### 4.2.1 Performance Improvement using GPU :

The Table.4.1. shows improvement in compute time for different sets of rate calculation iterated on GPU. Transferring of variables from CPU to GPU will have an overhead, but operations in GPU are much faster as operations are done in parallel using threads. So with increase in number of iterations gives better performance. The table is for rate calculations for a 95x95 matrices for powers and intensities of signal and pump using (95, 95) threads for 100$\mu$m space steps. The duration for CPU and GPU computation for 10, 100, 1000 and 10000 iterations and performance improvement using GPU is tabulated.

| No.of rate steps | Time on CPU(sec) | Time on GPU(sec) | Performance Improvement |
|---|---|---|---|
| 10 | 0.0096 | 0.00337 | 2.84x |
| 100 | 0.0946 | 0.0036 | 26.27x |
| 1000 | 0.9470 | 0.0183 | 51.74x |
| 10000 | 9.352 | 0.183 | 51.1x |

Table 4.1: Performance Improvement on GPU

It was identified that, parallel computation would be helpful in performance improvement when the overhead of information transfer between CPU and GPU is compensated by the improvement by GPU computation. This is much evident in case of calculations which require high computation on GPU like longer iterations.

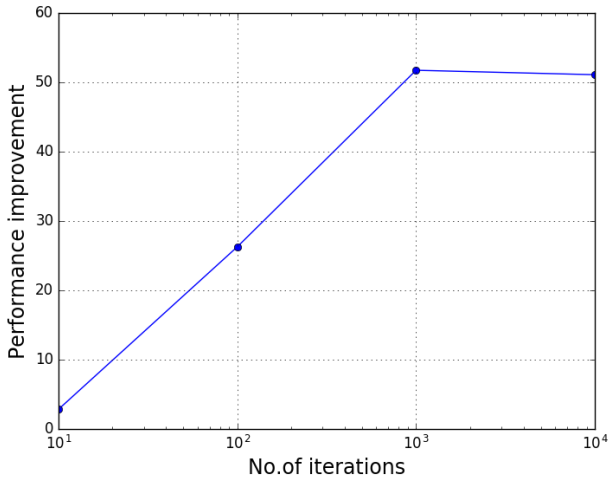


Figure 4.1: Improvement in performance for different iterations while using GPU instead of CPU

In our algorithm, the rate equations can be parallel computed using GPU as the power profiles are independent of the other grids. This allows use of multiple threads for each grid to improve performance. In current implementation, since the number of optical steps before a thermal calculation is around 40, the performance improvement using GPU would not be significant. Thermal calculations and eigenvalue calculations are not independent grid calculations making it difficult of parallelization. A different approach in this calculations will be required to improve the overall performance. In current implementation, the thermal calculation limits the speed of computation.

# Chapter 5

# Numerical experiments and results

A step index fiber with dimensions and properties was given in Table.5.1 was simulated. The model was run for fiber length of 1.63 m using the beam propagation method. Convergence of various numerical parameters including tolerance and space step was studied. The rate equation modelling was verified against the experimental results and RP simulations. The thermal solver was verified against the analytical solutions. The parameters used in the model, verification results and simulation results are described below.

## 5.1 Model Parameters

The parameters used in the model was similar to parameters from ref.[12].

| | |
|---|---|
| Number of grid points in the radial direction for thermal calculations | 383 |
| Number of grid points of the truncated region in the X and Y directions | 95 |
| Optical propagation step | $100\,\mu$m |
| Thermal propagation step | 4 mm |
| Core radius (a) | $37\,\mu$m |
| Inner cladding radius(b) | $85\,\mu$m |
| Outer claddingradius(c) | $200\,\mu$m |
| Permittivity of outer cladding | 2.0736 |
| Permittivity of inner cladding | 2.0740 |
| Permittivity of core | 2.0745 |
| Signal wavelength | $1.064\,\mu$m |
| Pump wavelength | $0.977\,\mu$m |
| Signal input power | 100 W |

| | |
|---|---|
| Pump Input power | 300 W |
| Upper state lifetime | $850\,\mu s$ |
| Signal Frequency | 281954887.21 MHz |
| Pump Frequency | 307062436.02 MHz |
| Signal emission cross section | $3.58 \times 10^{-25}\mathrm{m}^2$ |
| Signal absorption cross section | $6.00 \times 10^{-27}\mathrm{m}^2$ |
| Pump emission cross section | $1.87 \times 10^{-24}\mathrm{m}^2$ |
| Pump absorption cross section | $1.53 \times 10^{-24}\mathrm{m}^2$ |
| Yb dopant concentration | $3.5{\times}10^{25}\mathrm{m}^{-3}$ |
| Thermo-optic coefficient | $1.2 \times 10^{-5}\mathrm{K}^{-1}$ |
| Core and cladding thermal conductivity | 1.38 W/Km |
| Background Temperature | 300 K |

Table 5.1: Parameters used in the model

## 5.2 Verifications

The results obtained from the simulations were verified at different steps to ensure accuracy of the simulations. Convergence of various parametres used in the code was studied. The space step used for optical calculations and thermal calculations were studied to identify the convergence. The thermal steps were selected such that there is enough data points between each beat length, to study variation in different parameters with length.

The theoretical beat length of 24 mm was verified using simulations. The intensity variations in presence and absence of gain was studied at centre grid. The results obtained after rate calculations was verified against RP simulation data and experiments for various stages of experimental high power laser setup.

The numerical thermal calculations were verified against analytic equations [14]. The tolerance of thermal calculations were studied to find the appropriate tolerance.

### 5.2.1 Space step (dz) convergence

The convergence of space step was identified by varying the space step as 1cm, 1mm and $100\,\mu$m. The pump and signal power in an fiber amplifier of length 1.63 m was simulated using the rate equations for each of the space step. The results were plotted to identify the space step for which results converge. The results were found to converge for space step of 1 mm. $100\,\mu$m space step was used in the simulation for optical propagation calculation using the rate equations.

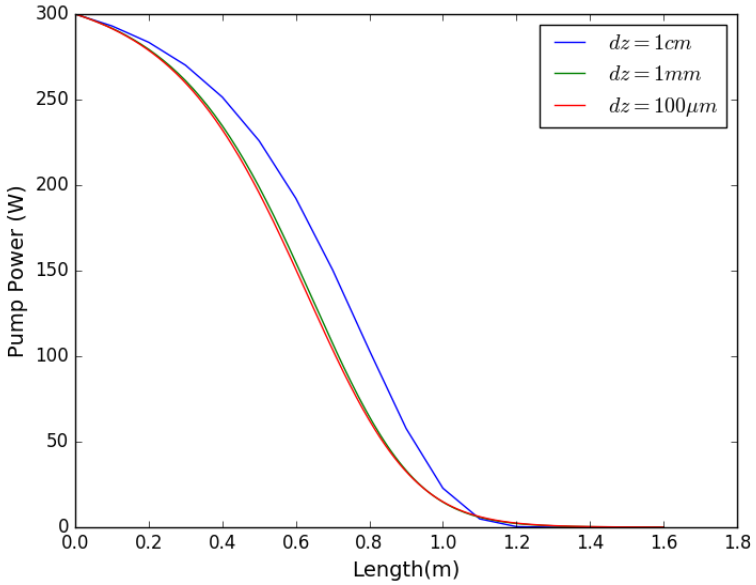


(a)

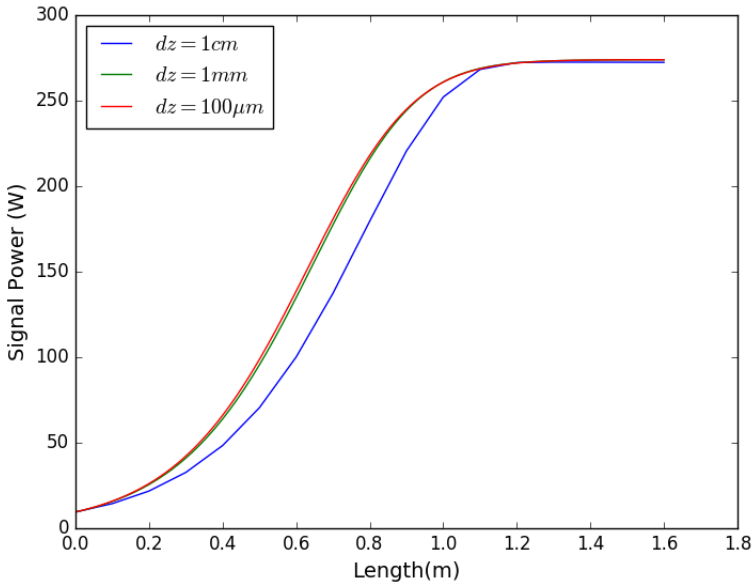


(b)

Figure 5.1: Convergence of optical space step: The (a) pump and (b) fundamental mode powers shown are the total power in the pump or fundamental mode in the cross-section calculated after propagating through space steps of 1cm, 1 mm and 100 $\mu$m

### 5.2.2 Intensity variations in presence and absence of gain

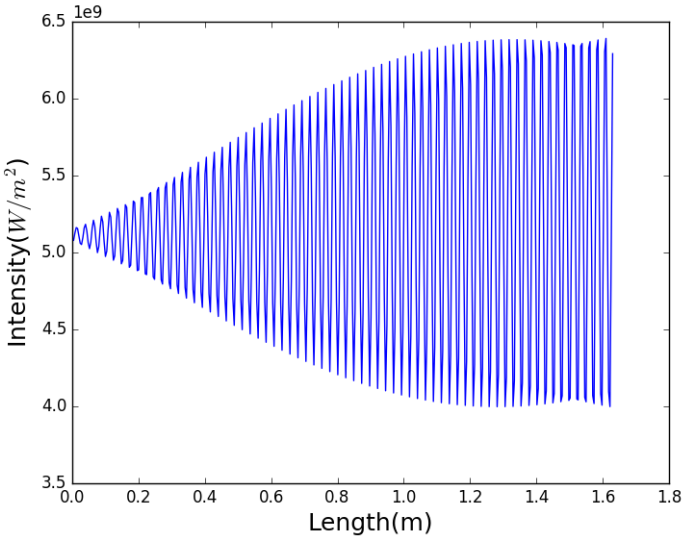


(a)

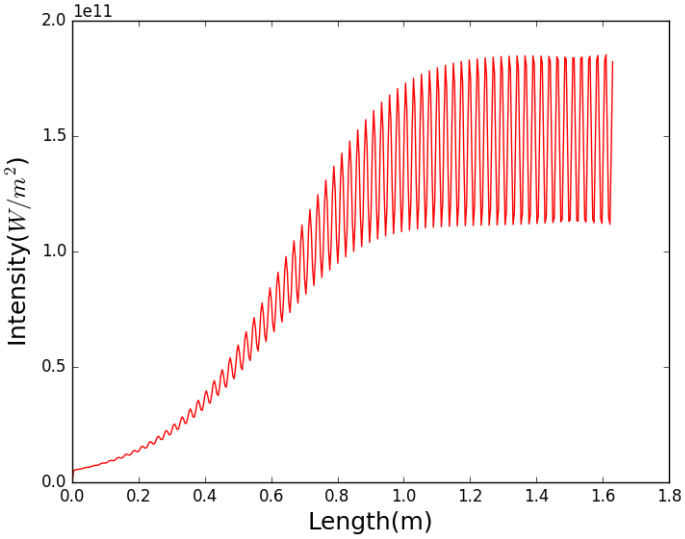


(b)

Figure 5.2: Intensity variation at an offset point 5 $\mu$m away from centre of fiber, calculated after space step of 4mm along length of the fiber in (a) absence and (b) presence of gain medium.

The intensity due to presence of multiple modes in the medium was studied along the length of the fiber in presence and absence of gain. Due to coherent interference of modes of the fiber, a beat length corresponding to difference in the propagation

constants is present along the length of fiber. A beat length of 24 mm was observed. Thermal step of 4 mm is considered such that there is atleast six points per beat length. This enables study of various parameters along the length of the fiber. The beating between these modes are visible at offset points rather than at the centre, due to dominance of fundamental mode with high intensity at the centre. At offset points the intensity due to higher order modes are comparable with that of fundamental mode which increases the visibility. Fig.5.2 shows the variation in intensity at an offset point $5\,\mu$m away from centre of fiber, calculated after space step of 4 mm along length of the fiber. An offset point is considered as the beat length is much evident at an offset point than at the centre.

### 5.2.3 Gain saturation for the modes

As shown in Fig.2.1, the input pump power of 300 W and signal power for $LP_{01}$,$LP_{11a}$, and $LP_{11b}$, are in saturation regime, causing gain saturation for the signal propagates along the fiber. Out of the 10 W input power, 9.5 W is excited as $LP_{01}$, mode and rest equally into $LP_{11a}$, and $LP_{11b}$. Due to high power in the $LP_{01}$, mode, the excited ion population is decided largely by this mode. The gain saturates faster at the centre of the fiber, due to presence of high power $LP_{01}$ mode. To the outer edges, where power in the fundamental mode is comparable with higher order mode, gain saturation is decided by the total signal intensity. This is because the frequency of all these modes are the same, and the medium cannot differentiate among this modes. Thus, the effect of gain saturation on the modes is thus solely due to the gain profile.

Due to higher power in fundamental mode, the gain available for this mode is lower than that of higher order mode. Thus the amplification seen by the fundamental mode along the length would be less than that of the higher order mode. This would result in slight increase in higher order mode power content compared to the fundamental mode as larger pump power would be transferred to the higher order mode.

### 5.2.4 Verification of results with experimental data

The simulation results were verified against the RP simulation results and experimental results obtained from experimental setup for high power laser with various stages. The power is increased in different stages to obtain the high power. The results match the experimental data. In stage II, the simulation results match the experimental data than the RP simulations.

Fig.5.3. shows the plots for verification of TMI simulation results against experimental data and RP simulation data for amplification through fiber amplifier. The

output signal power was plotted against different input pump power for various stages of high power laser setup. Stage I has input signal power of 36 mW amplified through 1.5 m fiber. Stage II and stage III have input signal powers of 90 mW and 2.26 W and are 5 m and 3.3 m long. The simulations in TMI code and RP Fiber Power software is done for space step of 100 $\mu$m.

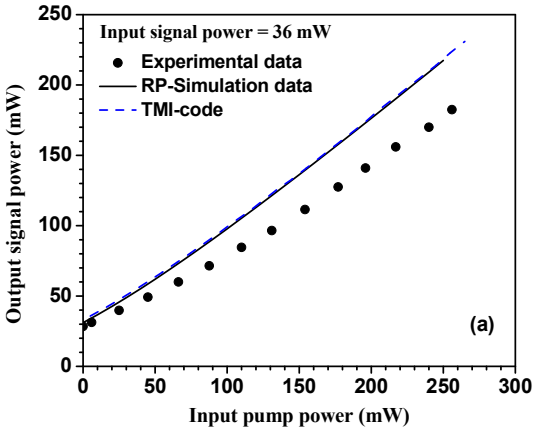


(a)

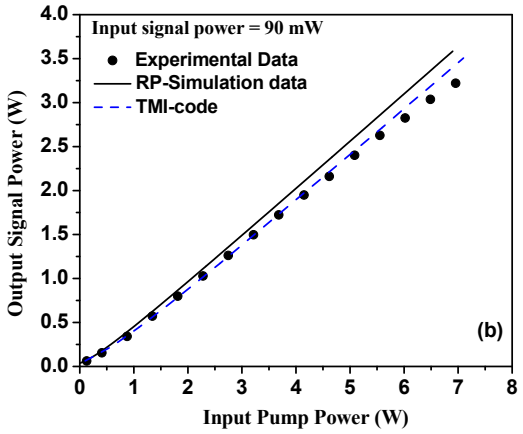


(b)

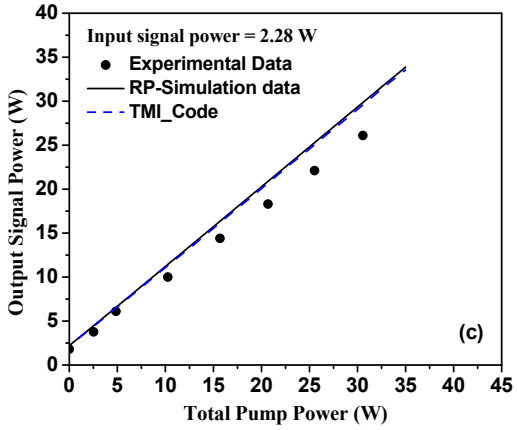


(c)

Figure 5.3: Verification of TMI code results against experimental data and RP simulation data : The output signal power was plotted against different input pump power for stage, input power and length of the fiber respectively in (a) stage I, 36 mW, 1.5 m; (b) stage II, 90mW, 5m and (c) stage III, 2.28 W, 3.3 m. The simulations in TMI code and RP Fiber Power software is done for space step of 100 $\mu$m.

### 5.2.5 Verification of thermal solver

A 2D thermal solver is used in the model to calculate the temperature variation inside the fiber due to absorption of signal by the medium. Finite difference method is implemented to solve the steady-state heat equation. The diffusion along the length of fiber was considered negligible. Uniform thermal conductivity was assumed across all directions of fiber.

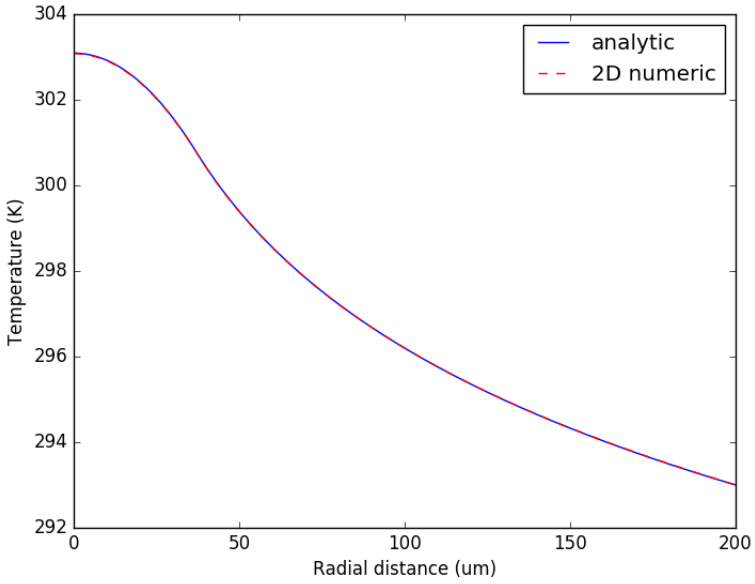


Figure 5.4: Verification of numerical thermal results against analytical solution for Dirichlet boundary condition : For a double-clad fiber cross-section with uniform thermal conductivity, the temperature variations along the radial direction with heat source of 40 W present in the core of the fiber was calculated for a tolerance of $10^{-8}$.

The steady-state thermal solver was verified against the analytical results in radial direction for Dirichlet boundary condition. The analytical solutions used is given in appendix. Tolerance of $10^{-8}$ was found to be appropriate for thermal calculation. The time taken for each thermal calculation was limited by this, which limited the overall performance of beam propagation model.

Fig.5.4. shows the temperature variations along the radial direction with heat source of 40W present in the core of the double-clad fiber calculated for a tolerance of $10^{-8}$. The analytical and numerical solutions converge for this tolerance. The verification was done using the steady-state heat equation in radial direction, which was latter used to verify the 2D numerical solution in cartesian coordinates.

**Diffusion in z direction :** The diffusion in z direction is usually neglected in thermal instability models. Feasibility of this assumption in our model was studied. A 3D thermal solver was used to solve for a 4 mm long cylinder with thermal properties similar to the double clad-fiber of 200 $\mu$m radius as used in the model. Two heat source of heat source of 40W was considered to be present at 750 $\mu$m and 2.5 mm with a heat sink of 300 K present around the cylinder. The results of steady-state 3D thermal calculation showed that the temperature diffuses back to background temperature of 300 K within 200 $\mu$m due to presence of heat sink in radial direction which absorbes the heat. This is shown in Fig.5.5 which shows the variation of temperature along length at the centre of cylinder. Thus neglecting z diffusion can be assumed when considering uniform thermal conductivity in all directions, allowing consideration of slices of fiber after 4 mm to be thermally independent.

Thus the model uses a 2D steady-state thermal solver with tolerance of $10^{-8}$ and Dirichlet boundary condition for temperature calculations.

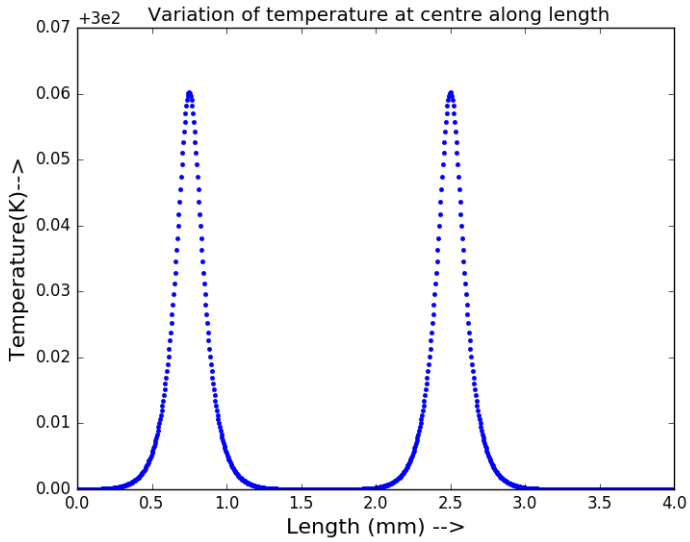


Figure 5.5: The variation of temperature along length at the centre of cylinder of radius 200 $\mu m$ placed in heat sink of 300 K with heat sources at 750 $\mu$m and 2.5 mm.

## 5.3 Comparison of output parameters in the presence and absence of thermo-optic effect

The signal and pump power in the fiber is studied in presence and absence of thermo-optic effect. Variation of parameters was studied and resultant physical conse-

quences were inferred.

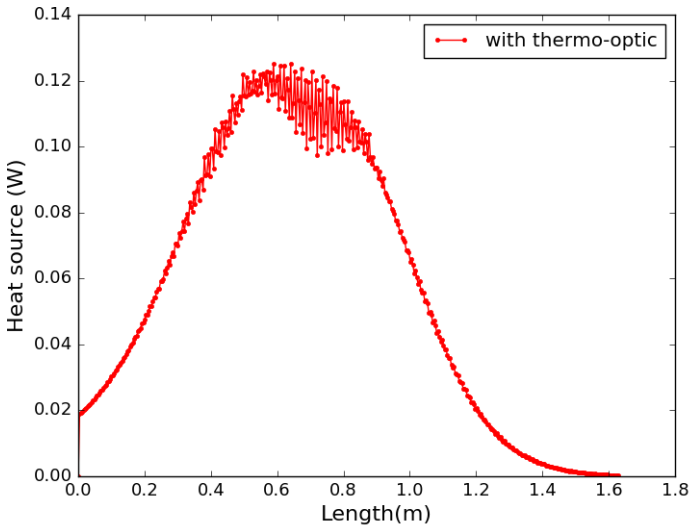


Figure 5.6: Heat source generated in fiber amplifier cross-section due to thermo-optic effect when optical space step of 100$\mu m$ and thermal space step of 4 mm is considered.

In the absence of thermo-optic effect, refractive index is uniform along the length of the fiber. The signal and pump pass through this active medium, amplifying the signal modes independently and completely absorbing the pump power by the end of the 1.63 m fiber. In this case, the modes propogate unperturbed and do not interact with each other.

When the thermo-optic effect is considered, the thermal gratings induce refractive index variations. The thermal grating formed depends on the gain as shown in Fig.5.6. The modes propagating through this perturbed medium, are no longer the eigenmodes of the system, thus coupling power between them. The fundamental mode couples energy to the higher order modes. The power in fundamental mode is much lower in presence of thermo-optic while the power in higher order mode is significantly higher. This further enhances the grating and result in formation of mode flucctuations Fig.5.7. shows the comparison of signal power in fundamental and higher order modes, change in refractive index and pump power along the length of fiber in presence and absence of the thermo-optic effects.

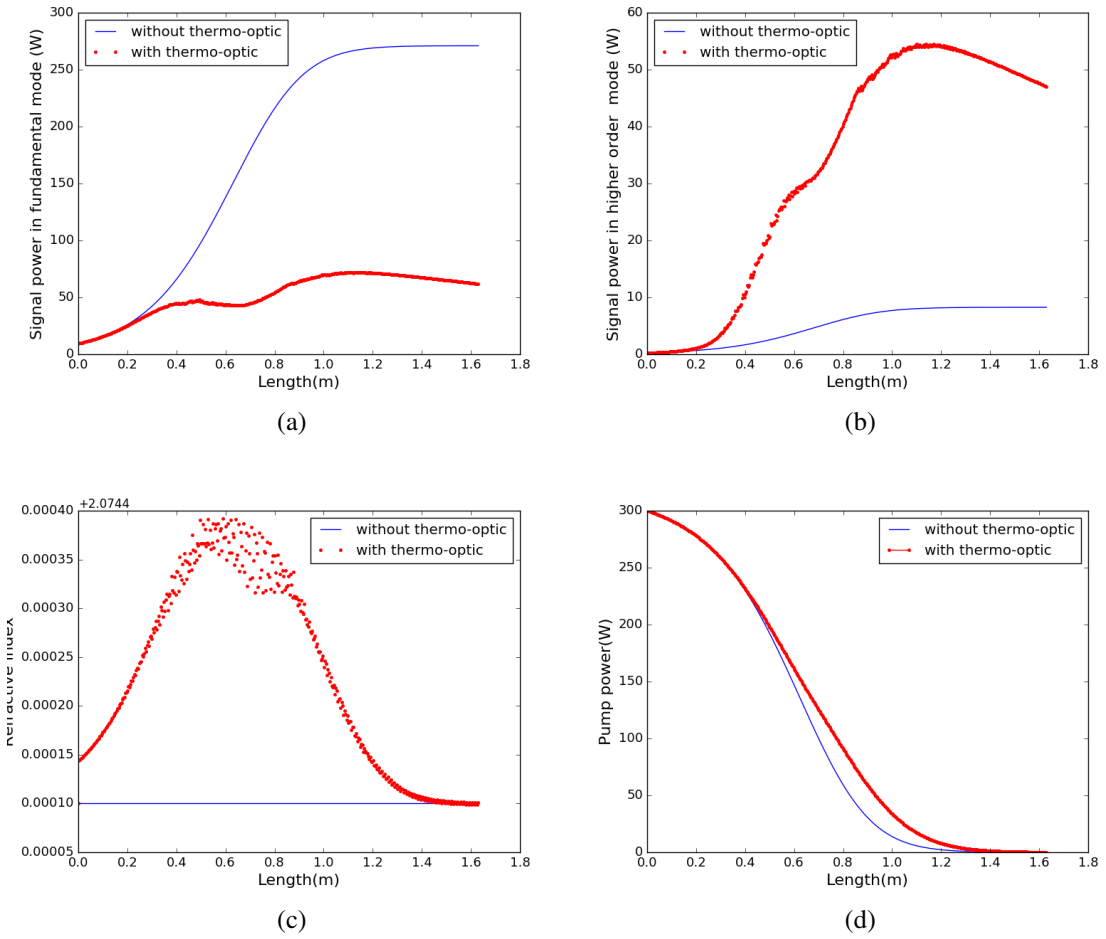


Figure 5.7: Comparing variation in (a) signal powers in fundamental mode, (b) higher order mode, (c) refractive index in centre grid and (d) pump power in presence and absence of thermo-optic effects, when optical space step of $100\mu m$ and thermal space step of 4 mm is used.

Temperature profile variation and refractive index grating along the length of the fiber is shown in Fig.5.8. The intensity which vary along the length with a beat length causes inversion and thus temperature profile variation in similar manner. Refractive index grating is formed by variation in refractive index profile through thermo-optic effect. When the beam propagating along the fiber core sees this perturbation, the modes cease to be the eigenmodes of the perturbed system resulting in power transfer to the perturbed and continue to propagate as the perturbed mode. In this fashion, the energy from fundamental mode gets transferred to higher order mode thus resulting in mode intensity profile variations. When this happen in presence of temporal grating, it result in beam fluctuations.

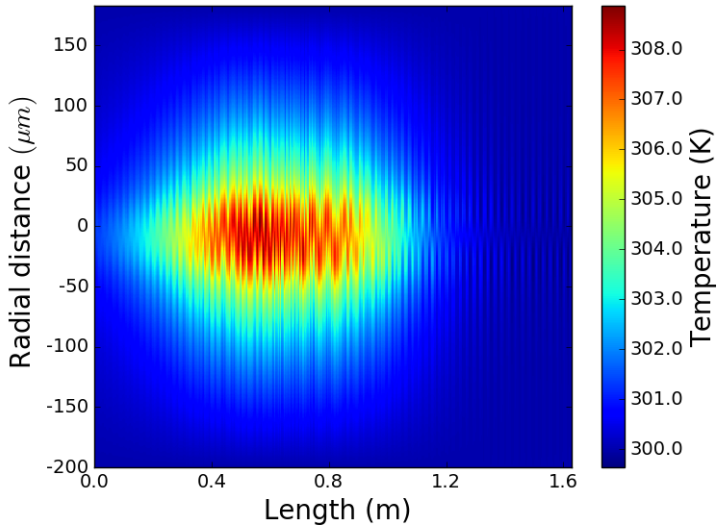


(a)

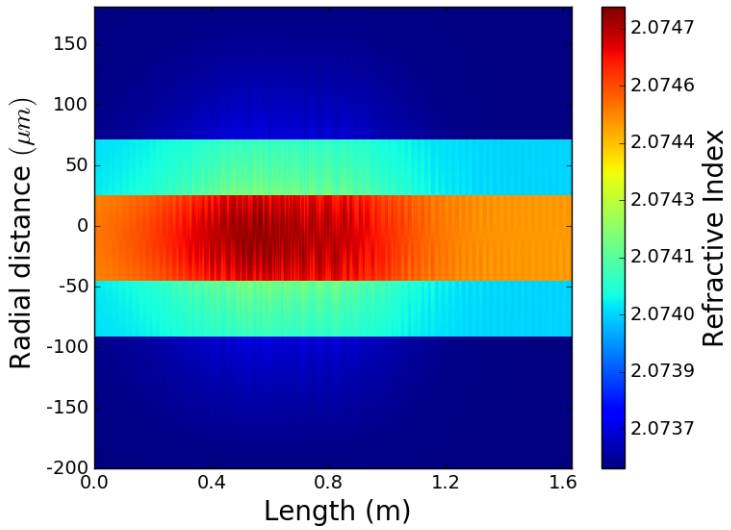


(b)

Figure 5.8: (a) Temperature and (b) refractive index profile along the longitudinal section of the fiber

## 5.4 Ratio of powers

In presence of thermal mode instabilities, the output fluctuate between the fundamental and higher order modes. Steady-state model would show power transfer from fundamental to higher order modes as signal propagates along the fiber in presence of thermal grating. The refractive index grating formed due to thermo-optic effect allows

mode coupling between otherwise orthogonal modes.

The ratio of input and output powers in presence and absence of thermo-optic effects were studied. The fractional mode content in each mode along the length of the fiber was plotted to study the power transfer between the modes.

| ***Signal power in*** | ***Input*** | | ***Output without thermo-optic*** | | ***Output with thermo-optic*** | |
|---|---|---|---|---|---|---|
| ***Fundamental mode*** | 9.5 W | 95% | 270.93 W | 94.26 % | 61.8 W | 39.64% |
| ***Higher order modes*** | 0.5 W | 5% | 16.5 W | 5.72% | 94.08 W | 60.35% |
| ***Ratio(FM:HOM)*** | 19.0 | | 16.42 | | 0.65 | |

Table 5.2: Ratio of powers at input and at output with absence and presence of thermo-optic effect

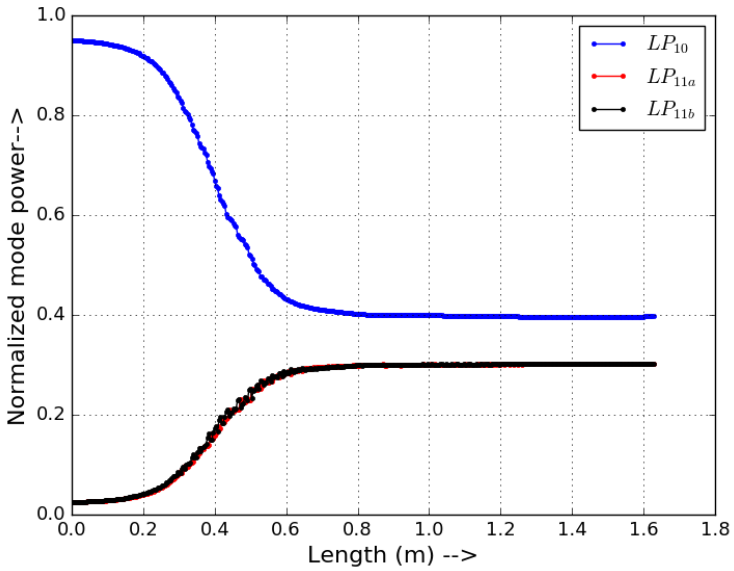


Figure 5.9: Normalized power in $LP_{01}$, $LP_{11a}$, and $LP_{11b}$, showing power transfer as the beam propagates in presence of thermo-optic effect along the length of fiber.

The fraction of power in higher order modes increases when themo - optic effect is considered. The power transfers from fundamental to higher order mode as signal propagates along the length of fiber in presence of thermal induced refractive index grating. Fig.5.9 shows the power transfer between the modes in presence of thermal grating, as the normalized power content in fundamental mode decreases with length while that in higher order mode increase with length.

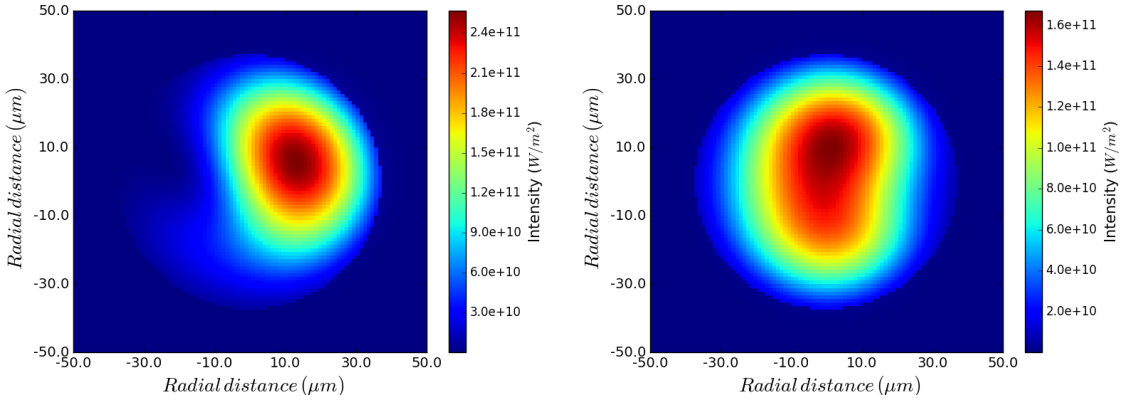


(a) Profile I (b) Profile II

Figure 5.10: Various intensity profiles at the cross-section towards the end of the fiber.

The current steady-state model successfully simulated the power transfer between modes which can cause temporal fluctuations in output beam of high power fiber laser in a transient model. As shown in Fig.5.10, to the end of the fiber, when the higher order mode power increases the intensity starts fluctuating. The net intensity of modes at the cross-section shows instability. Presence of these different profiles in a steady-state model, would be transferred to temporal flucctuations in modes in a transient model, thus leading to mode instabilities at high powers.

# Chapter 6

# Conclusion

## 6.1 Summary of work done

A steady-state model of thermal modal instability in fiber amplifiers has been presented. This model uses a 3D BPM combined with 2D thermal solver, to study thermal induced intensity fluctuations. The mode calculations were done using ARPACK package. The numerical solver was verified at different stages to ensure the accuracy of simulation. The scope of parallel computation to improve the performance of the model was studied.

Various physical phenomena that occur in high power fiber lasers were studied using the model. Gain saturation of the modes and thermal gratings formation which allow power coupling was observed. The physical origin of thermal mode instability was investigated using the model. The signal and pump propagation through the fiber in presence and absence of thermo-optic effect was studied. The refractive index increase with increase in temperature. Fundamental mode power and increase in higher order mode powers were observed in presence of thermo-optic effect. The steady state model used was able to simulate power transfer between the modes, which is the primary condition for thermal mode instability in high power fiber lasers.

## 6.2 Future scope

The model presented here enables numerous further investigations, of which a few are briefly discussed below.

A transient model is found to be neccessary to model temporal fluctuations in the output beam of high power fiber lasers due to thermal mode instabilities. A transient model which solves the time-dependent heat equation can study the different

time scales present in the phenomena. The speed of optical propagation and time diffusion need to be quantified to find the appropriate algorithm which will allow better scope for parrallel computing. This can also study the build up and decay times of the instability.

Although former models in this study could provide invaluable insights into the physics and origin of mode instabilities, they are generally too computationally intensive. This can hinder its ability to evaluate the impact of potential mitigation strategies effectively. For such a purpose, a quick and easy way of determining the threshold is preferable, eventhough it might sacrifices a certain degree of accuracy. A transient desktop model can be made possible using further inclusion relevant approximations and extensive mathematical and computational methods. Effective algorithms and parallel computational approach might help in this purpose. Better algorithms in eigenmode calculations and thermal solver which allow more parallel computations is required to improve the overall performance.

The hypothesis on physical origin of TMI is still unclear. Further experimental and theoretical work on this is neccessary to find mitigation strategies for TMI which currently limits the power scalability. Furthermore, this model did not predict TMI threshold and study different regimes of mode instabilities. TMI threshold prediction can be compared with experimental thresholds to quantify the accuracy of the model.

# Appendix A

## Analytical solutions for steady-state heat equation

The model for solving the heat distribution [16] in double clad fiber cross-section in radial direction is shown in Fig.1.

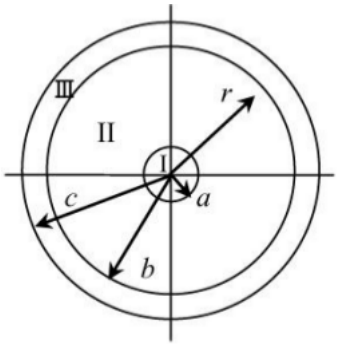


Figure A.1: Model for solving the temperature distribution of double clad-fiber cross-section (Ref:[16])

Applying the thermal conduction equation,

$$\frac{1}{r}\frac{\partial}{\partial r}[r\frac{\partial T(r)}{\partial r}] = \frac{-Q}{K} \tag{A.1}$$

where a,b,c are the core, inner cladding, and outer cladding radii, Q is the heat power density, and K is the thermal conductivity. Considering the continuity of temperatures and their derivatives at boundaries,

$$\frac{\partial T}{\partial r}\lfloor_{r=0} = 0 \tag{A.2}$$

$$k_3\frac{\partial T_3}{\partial r}\lfloor_{r=c} = h[T_c - T_3(r=c)] \tag{A.3}$$

where h is the convective heat transfer coefficient and $T_c$ the coolant temperature.

Applying these boundary conditions, the following analytical solutions were obtained in regions I, II and III.

$$T_0 = T_c + \frac{q_1 a^2}{2hc} + \frac{q_1 a^2}{4k_1} + \frac{q_1 a^2}{2k_2} ln(\frac{b}{a}) + \frac{q_1 a^2}{2k_3} ln(\frac{c}{b}) \tag{A.4}$$

$$T_3(r) = T_0 - \frac{q_1 a^2}{4k_1} - \frac{q_1 a^2}{2k_2} ln(\frac{b}{a}) - \frac{q_1 a^2}{2k_3} ln(\frac{r}{b}) \tag{A.5}$$

$$T_2(r) = T_0 - \frac{q_1 a^2}{4k_1} - \frac{q_1 a^2}{2k_2} ln(\frac{r}{a}) \tag{A.6}$$

$$T_1(r) = T_0 - \frac{q_1 r^2}{4k_1} \tag{A.7}$$

$T_0$ is the temperature at the centre. $T_1$, $T_2$, and $T_3$ are the temperatures in region I, II and III respectively.

# Bibliography


[1] Johan Nilsson, David.N.Payne, "High Power Fiber-lasers", Science 332: 921-922,(2011)

[2] L.D.DeLoach, S.A.Payne, L.L.Chase, L.K.Smith, W.L.Kway, and W. F. Krupke, "Evaluation of absorption and emission properties of Yb 3+ doped crystals for laser applications," IEEE J. Quantum Electron. , vol. 29, no. 4, pp. 1179–1191, (1993)

[3] Michalis N. Zervas and Christophe A. Codemard, "High Power Fiber Lasers: A Review," IEEE J. Quantum Electron. , vol. 20, no. 5, (2014)

[4] Cesar Jauregui, "High-power fibre lasers, a review article," Nature Photonics, (2013)

[5] J. J. Koponen et.al, "Photodarkening in ytterbium-doped silica fibers," SPIE Security & Defense Europe Symposium (2005)

[6] Arlee V. Smith, Jesse J. Smith, "Review of models of mode instability in fiber amplifiers," OSA (2013)

[7] A. V. Smith and J. J. Smith, "Mode instability in high power fiber amplifiers," Opt. Express 19(11), 10180– 10192 (2011)

[8] N. Andermahr and C. Fallnich, "Optically induced long-period fiber gratings for guided mode conversion in few-mode fibers," Opt. Express 18(5), 4411–4417 (2010),

[9] A. Yariv and A. P. Yeh, "Photonics: Optical Electronics in Modern Communications," 6th Edition, Oxford University Press, New York,(2007)

[10] K. R. Hansen, T. T. Alkeskjold, J. Broeng, and J. Lægsgaard, "Thermo-optical effects in high-power Ytterbium-doped fiber amplifiers,"Opt. Express 19(24), 23965–23980 (2011),

[11] K. R. Hansen, T. T. Alkeskjold, J. Broeng, and J. Lægsgaard, “Theoretical analysis of mode instability in high- power fiber amplifiers,” Opt. Express 21(2), 1944–1971 (2013),

[12] Ward, Benjamin G., ”Modeling of transient modal instability in fiber amplifiers.”, Optics express 21.10 , 12053-12067 (2013)

[13] C. Jauregui, T. Eidam, J. Limpert, and A. Tünnermann, “The impact of modal interference on the beam quality of high-power fiber amplifiers,” Opt. Express 19(4), 3258–3271 (2011),

[14] C. Jauregui, T. Eidam, H. J. Otto, F. Stutzki, F. Jansen, J. Limpert, and A. Tünnermann, “Physical origin of mode instabilities in high-power fiber laser systems,” Opt. Express 20(12), 12912–12925 (2012),

[15] David C. Brown et.al,”Thermal, Stress, and Thermo-Optic Effects in High Average Power Double-Clad Silica Fiber Lasers,” IEEE J. Quantum Electron. , vol. 37, no. 2, 207-218, (2001)

[16] Y. Fan, Bing He et.al, ”Thermal effects in kilowatt all-fiber MOPA,” Opt. Express 19(16),15152-15174 (2011)